Wind and Structures, Vol. 14, No. 4 (2011) 359-381
DOI: http://dx.doi.org/10.12989/was.2011.14.4.359

Simplified formulations for flutter instability analysis of bridge deck

Tan-Van Vu[1], Young-Min Kim[2], Tong-Seok Han[3] and Hak-Eun Lee*[4]

[1.4]*School of Civil, Environmental and Architectural Engineering, Korea University, Seoul, South Korea*
[2]*Institute of Construction Technology, DAEWOO E&C Co., Ltd., Suwon, South Korea*
[3]*School of Civil and Environmental Engineering, Yonsei University, Seoul, South Korea*

(Received May 11, 2010, Accepted January 8, 2011)

Abstract. This paper deals with the flutter instability problem of flexible bridge decks in the framework of bimodal-coupled aeroelastic bridge system analysis. Based on the analysis of coefficients of the polynomials deduced from the singularity conditions of an integral wind-structure impedance matrix, a set of simplified formulations for calculating the critical wind velocity and coupled frequency are presented. Several case studies are discussed and comparisons with available approximated approaches are made and presented, along with a conventional complex eigenvalue analysis and numerical results. From the results, it is found that the formulas that are presented in this study are applicable to a variety of bridge cross sections that are not only prone to coupled-mode but also to single-mode-dominated flutter.

Keywords: bridges; eigenvalue; flutter; flutter derivatives; instability; simplified formulations.

1. Introduction

Long-span bridges are slender, low damping and flexible large-scale line-like structures that are very susceptible to wind loads. The excitation mechanisms for aeroelastic interaction between wind flow and structures may be distinguished as follows: extraneous-flow-induced excitations, flow-instability-induced excitations and movement-induced excitations. The latter excitation mechanism is caused by fluctuating wind forces due to movements of the vibrating structural part. Small deviations from the equilibrium position of the structure induce a re-distribution of impacting wind forces, which further increase the initial disturbances. If these self-excited forces lead to a negative damping threshold, the onset of flutter will occur and this directly induces structural failure, as was the case in the collapse of the Tacoma Narrows Bridge in 1940. In streamlined bodies such as airfoils, flutter occurs from a coupling of simultaneous vertical and torsional motion of which the frequencies are in phase with one another. This type of flutter is a two degree-of-freedom or coupled flutter, which was the cause of collapse of the Samuel Brown's Brighton Chain Pier. For a bluff body such as a plate girder, flutter occurs from a single degree-of-freedom, which is heaving-mode aeroelastic instability or torsional flutter. Heaving-mode aeroelastic instability was the cause of wild oscillation of the Deer Isle Bridge in 1942, while torsional flutter was the cause of the damage that occurred in 1826 to Telford's Menail Bridge (Scott 2001).

* Corresponding Author, Professor, E-mail: helee@korea.ac.kr

Since these events, the importance of flutter analysis of long-span bridges has been strongly recognized and has led to many research works and investigations on bridge aerodynamics. Early pioneering work on bridge flutter analysis was presented by Bleich (1949), where stiffness-driven flutter was addressed using airfoil aerodynamics theory. However, a wind speed with a value higher than that, which occurred for the Tacoma disasters, was given in this approach. While Selberg (1961) and Rocard (1963) proposed simplified empirical formulas for estimating flutter onset velocity, these formulas nevertheless are only rigorously applied for a flat plate section.

From the point of view of aerodynamics, Scanlan and Tomko (1971) mathematically described the self-excited forces in terms of flutter derivatives in the frequency-domain and offered an analysis on bridge flutter. Recently, the aerodynamic instability problem of long-span bridges can be analyzed by linear and nonlinear flutter approaches. Normally, the geometric nonlinearity of bridge structures and effects of nonlinear wind-structure interaction are neglected in the linear flutter approach. Nonlinear flutter analysis can be performed on the deformed configuration of bridge structures under the static wind action as suggested by previous authors (e.g., Zhang 2006).

In frequency domain, the linear flutter analysis methods can be grouped into two broad categories as follows: the mode-by-mode and multimode-coupled approach. The multimode-coupled approach is often performed by using aerodynamic coupling of fundamental vertical bending and torsional modes with secondary contributions from other modes. Hence, bimodal-coupled flutter analysis consisting of two fundamental modes remains a useful tool for an expeditious evaluation of bridge flutter performance at the preliminary design stage.

In the framework of binary flutter analysis, Nakamura (1978) suggested a set of approximated formulas based on theoretical assumptions about the unsteady aeroelastic behavior of bridge decks, in order to provide the frequency and rate of growth of oscillation, the position of the equivalent center of rotation and the phase difference between bending and torsion near the critical flutter point in the case of a variety of deck sections. Subsequently, Matsumoto (1999) proposed a step-by-step iterative method attempting to highlight the characteristics of the torsional and heaving branch at flutter onset. Based on closed-form solutions while assuming low-level damping, Chen and Kareem (2007) introduced an approximated formula of which only H_3^*, A_1^*, A_2^* and A_3^* flutter derivatives are needed to estimate the critical wind speed. From a manipulated and simplified process of the equation of the eigenvalue problem, Bartoli and Mannini (2008) presented analytical expressions for calculating critical frequency and reduced wind speed of which only H_1^*, $A_2^*$and A_3^* flutter derivatives are used, and these were also applied in the case of a section prone to torsional flutter. Accordingly, the approximated formulas can be successfully employed for capturing the physics of flutter mechanisms such as stiffness-driven flutter or damping-driven mechanisms for the given bridge deck section. Nevertheless, the limitation of these approaches is their inability to give reasonable results when the frequency ratio tends to unity and even in zero-damping condition, as well as in the case of cross sections that are prone to heaving-mode aeroelastic instability.

In the present paper, using an analysis process for coefficients of the polynomials deduced from singularity conditions of an integral wind-structure impedance matrix, a simplified formulation is presented in terms of flutter derivatives for calculating the critical wind velocity and coupled frequency. Because the uncoupled and coupled flutter derivatives remain in the simplified formulas, this considered framework seems to give reasonable results even if the frequency ratio is very close to unity in the case of low damping. Furthermore, if the coefficients of non-dimensional mass and moment of inertia associated with flutter derivatives were considered small or negligible, the simplified formulas, which only consist of fully uncoupled flutter derivatives (H_1^*, H_4^* and A_2^*, A_3^*)

extracted from the experimental system of 1-DOF sectional models, would no longer be tedious. However, the proposed simplified formulation is still able to be effectively applied for a bridge section that is not only prone to coupled-mode flutter but also single-mode instability (either dominated by torsion or heaving mode).

In the second section of this paper, a mechanical model is introduced to deal with the bimodal flutter problem and its solution is reviewed. Subsequently, simplified strategies are introduced, as the results of the approximated formulations consisting of the flutter derivatives are constructed in the third section. Finally, some results of numerical examples showing good agreement with those obtained via other approximated formulas as well as with the conventional complex eigenvalue analysis (CEA).

2. Bimodal approach to flutter problem

The natural circular frequencies of the first vertical bending and torsional modes in the aeroelastic bridge system are denoted as ω_z and ω_θ, respectively. Only aerodynamic forces generally dominate the aerodynamic performance of the bridge. The self-excited lift and pitching moment acting on the bridge deck section per unit length are given by Simiu and Scanlan(1996)

$$L^{ae}(t,K) = \frac{\rho V^2 B}{2}\left[KH_1^*\frac{\dot{z}}{V} + KH_2^*\frac{B\dot{\theta}}{V} + K^2H_3^*\theta + K^2H_4^*\frac{z}{B}\right] \tag{1}$$

$$M^{ae}(t,K) = \frac{\rho V^2 B}{2}\left[KA_1^*\frac{\dot{z}}{V} + KA_2^*\frac{B\dot{\theta}}{V} + K^2A_3^*\theta + K^2A_4^*\frac{z}{B}\right] \tag{2}$$

where z and θ are the vertical and torsional displacements, V = mean wind speed, B = bridge deck (Fig. 1), ρ = air density, the reduced frequency $K = 2k = \omega B/V$, and $H_i^*, A_i^* (i = \overline{1,4})$ = flutter derivatives, which are functions of reduced frequency and can be extracted from a wind-tunnel test. The governing equations of the combined bridge system in terms of the generalized modal coordinates η under approaching crosswind flow are expressed as

$$\boldsymbol{M}\ddot{\eta} + \boldsymbol{C}\dot{\eta} + \boldsymbol{K}\eta = \boldsymbol{F}^{ae} \tag{3}$$

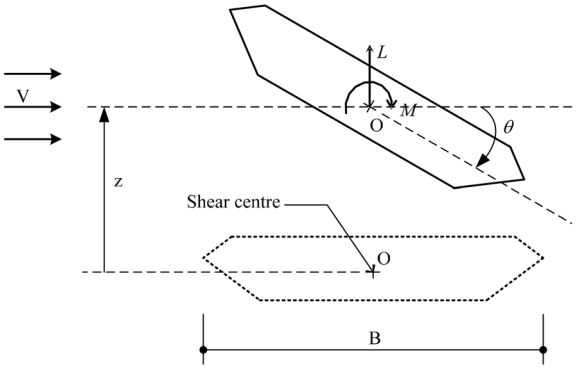

Fig. 1 Sign convention for the displacements and self-excited forces

where $\boldsymbol{M}$, $\boldsymbol{C}$, $\boldsymbol{K}$ are generalized modal mass, damping and stiffness matrices, respectively; $\boldsymbol{F}^{ae}$is the generalized self-excited force vectors and the over-dot denotes partial differentiation with respect to time. Taking the Fourier transform on both sides of Eq. (3) leads to Eq. (4), which is considered as the modal equilibrium equation of motion in the frequency domain (Strømmen 2006),

$$(-\boldsymbol{M}\omega^2 + i\boldsymbol{C}\omega + \boldsymbol{K})\boldsymbol{X}_\eta(\omega) = (i\boldsymbol{C}^{ae}\omega + \boldsymbol{K}^{ae})\boldsymbol{X}_\eta(\omega) \tag{4}$$

where $i^2 = -1$, matrices of $\mathbf{C}^{ae}$ and $\mathbf{K}^{ae}$ contain the coefficients that are required for the vertical and torsional motions. These coefficients are normalized by $\rho B^2\omega/2$ and $\rho B^4\omega/2$, wherein ω is the in-wind frequency dependent on mean wind velocity (V)

$$\boldsymbol{C}^{ae} = \frac{\rho B^2\omega}{2}\begin{bmatrix} H_1^* & BH_2^* \\ BA_1^* & B^2A_2^* \end{bmatrix},\ \boldsymbol{K}^{ae} = \frac{\rho B^2\omega^2}{2}\begin{bmatrix} H_4^* & BH_3^* \\ BA_4^* & B^2A_3^* \end{bmatrix} \tag{5}$$

The impedance matrix (Strømmen, 2006) can be obtained by,

$$[\boldsymbol{S}_\eta(\omega_r, V)] = \begin{bmatrix} 1-\kappa_{zz}^{ae} & -\kappa_{z\theta}^{ae} \\ -\kappa_{\theta z}^{ae} & 1-\kappa_{\theta\theta}^{ae} \end{bmatrix} - \begin{bmatrix} \left(\frac{\omega_r}{\omega_z}\right)^2 & 0 \\ 0 & \left(\frac{\omega_r}{\omega_\theta}\right)^2 \end{bmatrix} + i2\begin{bmatrix} \frac{\omega_r}{\omega_z} & 0 \\ 0 & \frac{\omega_r}{\omega_\theta} \end{bmatrix} \times \begin{bmatrix} \zeta_z - \zeta_{zz}^{ae} & -\zeta_{z\theta}^{ae} \\ -\zeta_{\theta z}^{ae} & \zeta_\theta - \zeta_{\theta\theta}^{ae} \end{bmatrix} \tag{6}$$

With

$$\kappa_{zz}^{ae} = \frac{\rho B^2}{2\tilde{m}_z}\left(\frac{\omega_r}{\omega_z}\right)^2 H_4^* G_{\phi_z\phi_z,\phi_z},\quad \kappa_{z\theta}^{ae} = \frac{\rho B^3}{2\tilde{m}_z}\left(\frac{\omega_r}{\omega_z}\right)^2 H_3^* G_{\phi_\phi\phi_\phi,\phi_\phi},\quad \kappa_{\theta z}^{ae} = \frac{\rho B^3}{2\tilde{m}_\theta}\left(\frac{\omega_r}{\omega_\theta}\right)^2 A_4^* G_{\phi_\theta\phi_z,\phi_z}$$

$$\kappa_{\theta\theta}^{ae} = \frac{\rho B^4}{2\tilde{m}_\theta}\left(\frac{\omega_r}{\omega_\theta}\right)^2 A_3^* G_{\phi_\theta\phi_\theta,\phi_\theta},\quad \zeta_{zz}^{ae} = \frac{\rho B^2}{4\tilde{m}_z}\left(\frac{\omega_r}{\omega_z}\right) H_1^* G_{\phi_z\phi_z,\phi_z},\quad \zeta_{z\theta}^{ae} = \frac{\rho B^3}{4\tilde{m}_z}\left(\frac{\omega_r}{\omega_z}\right) H_2^* G_{\phi_z\phi_\theta,\phi_z}$$

$$\zeta_{\theta z}^{ae} = \frac{\rho B^3}{4\tilde{m}_\theta}\left(\frac{\omega_r}{\omega_\theta}\right) A_1^* G_{\phi_\theta\phi_z,\phi_\theta},\quad \zeta_{\theta\theta}^{ae} = \frac{\rho B^4}{4\tilde{m}_\theta}\left(\frac{\omega_r}{\omega_\theta}\right) A_2^* G_{\phi_\theta\phi_\theta,\phi_\theta},\quad G_{\phi_m\phi_n,\phi_p} = \int_{L_{exp}} \phi_m\phi_n dx \Big/ \int_L \phi_p^2 dx$$

where $G_{\phi_m\phi_n,\phi_p}[m,n,p=(z,\theta)]$ are modal integrals; $\tilde{m}_z$ and $\tilde{m}_\theta$ are the modal mass associated with the vertical and torsional modes; L and L_{exp} are length and wind exposed lengths. The effects of ζ_{xy}^{ae} and $\kappa_{xy}^{ae}(x, y = z, \theta)$ change the damping and stiffness properties of the combined bridge system, respectively.

Introducing the simplifications of $L_{\text{exp}} = L$ and $\phi_z = \phi_\theta$, any stability limit can be found by setting the determinant of the coefficient matrix of Eq. (6) equal to zero, resulting in cubic or quartic polynomials in the real or imaginary parts with respect to the in-wind frequency ratio Ω as follows,

$$\gamma^2\left[1 + \frac{1}{2}(\lambda_z H_4^* + \lambda_\theta A_3^*) + \frac{\lambda_z\lambda_\theta}{4}(A_1^*H_2^* - A_2^*H_1^* + A_3^*H_4^* - A_4^*H_3^*)\right]\Omega^4 + \gamma(\gamma\zeta_\theta\lambda_z H_1^* + \zeta_z\lambda_\theta A_2^*)\Omega^3 -$$
$$-\left[1 + \gamma^2 + 4\gamma\zeta_\theta\zeta_z + \frac{1}{2}(\lambda_z\gamma^2 H_4^* + \lambda_\theta A_3^*)\right]\Omega^2 + 1 = 0 \tag{7}$$

$$\gamma^2\left[\frac{1}{2}(\lambda_z H_1^* + \lambda_\theta A_2^*) + \frac{\lambda_z\lambda_\theta}{4}(H_1^*A_3^* - H_2^*A_4^* - H_3^*A_1^* + H_4^*A_2^*)\right]\Omega^3$$
$$-2\left[\zeta_z\left(\frac{\lambda_\theta}{2}A_3^* + \gamma\right) + \gamma^2\zeta_\theta\left(\frac{\lambda_z}{2}H_4^* + 1\right)\right]\Omega^2 - \frac{1}{2}(\lambda_z\gamma^2 H_1^* + \lambda_\theta^* A_2^*)\Omega + 2(\zeta_z\gamma + \zeta_\theta) = 0 \quad (8)$$

where $\gamma = \omega_\theta/\omega_z$ is the structural frequency ratio; $\lambda_z = \rho B^2/\tilde{m}_z$ and $\lambda_\theta = \rho B^4/\tilde{m}_\theta$ represent the non-dimensional mass and the polar moment of inertia, respectively; $\Omega = \omega_r/\omega_\theta$ is the in-wind frequency ratio for bridge sections prone to coupled flutter and is expressed as follows,

$$1/\gamma \le \Omega \le 1 \quad (9)$$

It can be seen that the solution of these equations requires searching for the lowest identical roots with respect to Ω, which do not easily allow practical calculation by hand, from both the fourth and third degree polynomial. Moreover, if this analysis is performed, it is rather difficult to identify in which branch the coupled flutter instability occurs. This is because the formula to determine the in-wind frequency ratio, Ω for a torsional and heaving branch is symmetric in terms of torsional and heaving motion.

3. Approximated solutions to bimodal flutter problem

3.1. Approximated 2-DOF flutter derivatives formulations

In order to simplify the bimodal flutter equation, let us set the coefficients of the fourth order polynomial obtained by imposing the vanishing of the real part from the determinant of the impedance matrix in Eq. (7) as follows

$$R_1 = \gamma^2\left[1 + \frac{1}{2}(\lambda_z H_4^* + \lambda_\theta A_3^*) + \frac{\lambda_z\lambda_\theta}{4}C_R\right] \quad (10a)$$

$$R_2 = \gamma\,(\gamma\zeta_\theta\lambda_z H_1^* + \zeta_z\lambda_\theta A_2^*) \quad (10b)$$

$$R_3 = -\left[1 + \gamma^2 + 4\gamma\zeta_\theta\zeta_z + \frac{1}{2}(\lambda_z\gamma^2 H_4^* + \lambda_\theta A_3^*)\right] \quad (10c)$$

where $C_R = -H_1^*A_2^* + H_2^*A_1^* - H_3^*A_4^* + H_4^*A_3^*$

For an analogous reason, Eq. (8) obtained by imposing the vanishing of the image part from the determinant of the impedance matrix, the setting coefficients are as follows

$$I_1 = \gamma^2\left[\frac{1}{2}(\lambda_z H_1^* + \lambda_\theta A_2^*) + \frac{\lambda_z\lambda_\theta}{4}C_I\right] \quad (11a)$$

$$I_2 = -2\left[\zeta_z\left(\frac{\lambda_\theta}{2}A_3^* + \gamma\right) + \gamma^2\zeta_\theta\left(\frac{\lambda_z}{2}H_4^* + 1\right)\right] \quad (11b)$$

$$I_3 = -\frac{1}{2}(\lambda_z\gamma^2 H_1^* + \lambda_\theta A_2^*) \quad (11c)$$

$$I_4 = 2(\zeta_z \gamma + \zeta_\theta) \tag{11d}$$

where $C_I = H_1^* A_3^* - H_2^* A_4^* - H_3^* A_1^* - H_4^* A_2^*$

Once the terms of $I_i = (i = 1, \ldots, 4)$ and $R_j (j = 1, \ldots, 3)$ are introduced, Eqs. (7) and (8) can be rewritten as follows

$$I_1 \Omega^3 + I_2 \Omega^2 + I_3 \Omega + I_4 = 0 \tag{12}$$

$$R_1 \Omega^4 + R_2 \Omega^3 + R_3 \Omega^2 + 1 = 0 \tag{13}$$

In the design of cable-supported bridges, three basic section configurations bluff girder, streamlined box and slotted girder sections, are widely used in the design (Yang and Ge 2009). Hence, it is important to analyze dynamic and aerodynamic parameters from existing bridges with three sections to derive the approximated formulas. Table 1 summarizes the data of four Edge girder bridge sections with dimensions and cross sections taken into account: Busan-Geoge Bridge (Lee *et al.* 2004), Seohae Grand Bridge (KHC 1998), Kärkinen (Kiviluoma 2001), and Golden Gate (Simiu and Scanlan 1996). Data of the streamline bridge sections is shown in the second part of the Table 1: Great Belt Bridge (Larsen 1993, Nissen *et al.* 2004), 2nd Geo-Germ Bridge (Larsen 2002), Hoga Kusten Bridge (Livesey 1995), Tsurumi Fairway Bridge (Sarkar *et al.* 1992). At the end of the table, three slotted girder bridge sections are considered: Messina Straits Bridge (D'Asdia and Sepe 1998), Xihoumen Bridge (Yang *et al.* 2007) and Shanghai Bridge (Zhou and Ge 2009).

From the data gathered in the last three columns of Table 1, it can be seen that the value of non-dimensional mass is smaller than that of the moment of inertia. Furthermore, the value of the free term I_4 in Eq. (12) is much smaller than unity. In addition to investigating the impact of terms in

Table 1 Geometric and dynamics properties with coefficient of I_4 of the different bridges

	$B\,(m)$	$f_z\,(Hz)$	γ	$\zeta_z = \zeta_\theta$	$\tilde{m}_z(kg/m)$	$\tilde{m}_\theta(kgm^2/m)$	λ_z	λ_θ	I_4
Edge girder bridge section									
Busan-Geoge Grand	22.0	0.334	3.00	0.005	26,854	1,430,000	0.023	0.205	0.0400
Seohae Grand	34.0	0.250	1.84	0.005	28,789	2,756,000	0.050	0.606	0.0284
K$\ddot{a}$rkinen	13.28	0.4646	1.51	0.0064	17,193	306,218	0.013	0.127	0.0321
Golden Gate	27.5	0.1638	1.17	0.005	5,208	3,680,000	0.182	0.194	0.0217
Streamline bridge section									
Great Belt	31.0	0.099	2.75	0.005	22,700	2,470,000	0.053	0.467	0.0375
2nd Geo-Germ	16.9	0.185	2.99	0.003	11,699	295,250	0.031	0.345	0.0240
Hoga Kusten	22.0	0.1198	2.10	0.005	10,588	603,209	0.057	0.485	0.0310
Tsurumi	38.0	0.204	2.38	0.005	32,220	2,880,100	0.056	0.905	0.0338
Slotted box girder bridge section									
Messina Straits	60.4	0.0605	1.32	0.01	55,000	28,000,000	0.083	0.594	0.0463
Xihoumen	36.0	0.1005	2.31	0.01	27,511	4,002,800	0.059	0.525	0.0662
Shanghai	51.5	0.2520	2.64	0.005	35,151	10,076,000	0.094	0.873	0.0364

Eqs. (12) and (13) on their own, let us take into account the aerodynamic behavior of two groups of the bridge deck section, one of these groups consists of two bridge deck sections that are quite different from each other: the thin flat plate (Theodorsen 1934) and the rectangular sections with width to depth ratio of B/D = 15, $R15$ (Matsumoto 1996); another of these groups consisting of two bridge deck sections are often used in super long bridges: section of 2TF and 2TFGP (Matsumoto *et al.* 2004).

For several levels of reduced wind velocity of V/fB, these terms that are gathered in groups are calculated in the case of low ($\zeta_z = \zeta_z = 0.0025$) and high level damping ratios ($\zeta_z = \zeta_\theta = 0.01$). Furthermore, this investigation is also performed on sets of structural frequency ratios with the case of the fundamental vertical bending frequency close to torsional frequency (case of Golden Gate bridge, $\gamma = 1.17$) and vice versa (case of Kärkinen bride, $\gamma = 1.51$), both of which are in the in-wind frequency ratios of $\Omega = 0.95$; other sets of in-wind frequency ratios around the flutter onset ($\Omega = 0.80$ and $\Omega = 0.85$) that satisfied the inequality (9) for the section of 2TF, 2TFGP with theirs structural frequency ratio assumed are 1.72 and 1.30, respectively.

Finally, the results obtained from the mentioned cases are presented in the form of graphs in order to

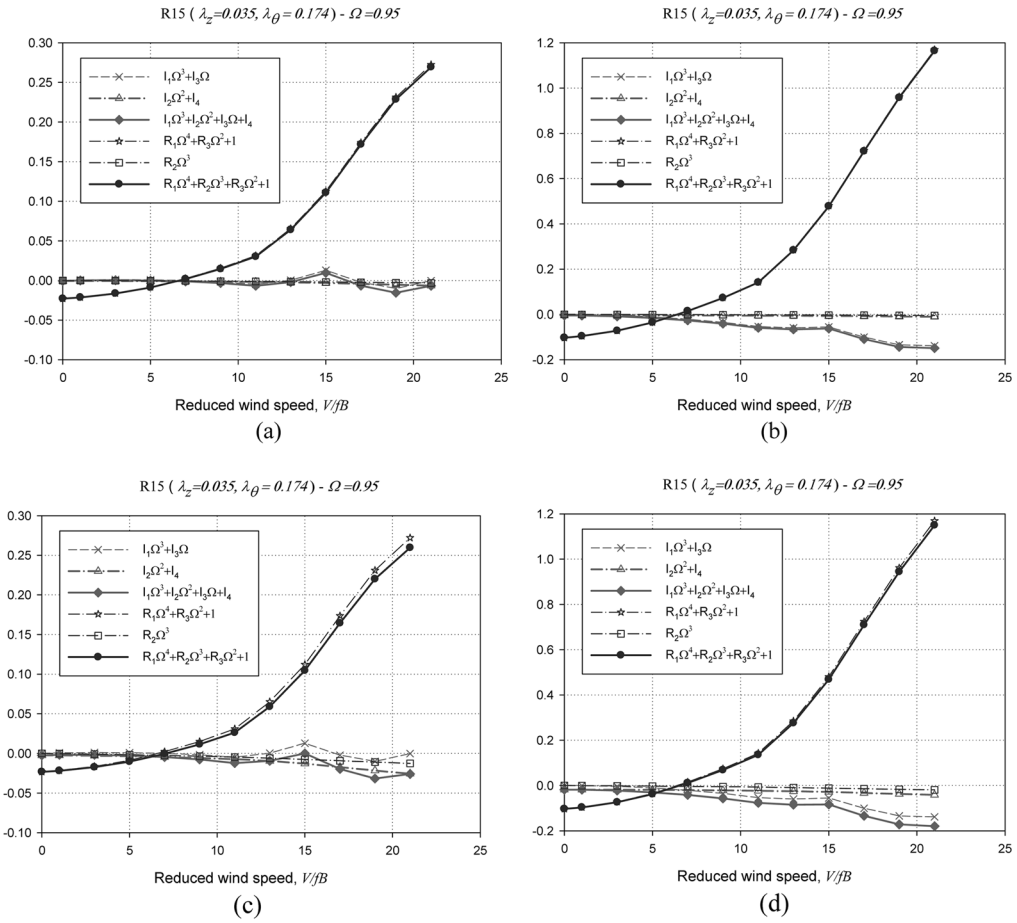

Fig. 2 Variation in R_i, I_i of R15 with V/fB
(a) $\zeta_z = \zeta_\theta = 0.0025$, $\gamma = 1.17$, (b)$\zeta_z = \zeta_\theta = 0.0025$, $\gamma = 1.51$,
(c) $\zeta_z = \zeta_\alpha = 0.01$, $\gamma = 1.17$ and (d) $\zeta_z = \zeta_\alpha = 0.01$, $\gamma = 1.51$

facilitate comparisons. For example, Fig. 2 for the rectangular section of R15 (λ_z = 0.035, λ_θ = 0.174); Fig. 3 for the theoretical thin Flat Plate section (λ_z = 0.027, λ_θ = 0.163) ; Fig. 4 for the 2*TF* section λ_z = 0.023, λ_θ = 0.143; Fig. 5 for the 2*TFGP* section (λ_z = 0.027, λ_θ = 0.163). It is evident that the term $R_2\Omega^3$ is definitely negligible with respect to the other terms in Eq. (13). The results from figures show that the value of Eq. (12) is dependent on the sum of the terms $I_1\Omega^3$ and $I_3\Omega$ in case of the low damping ratios. Nevertheless, several linear differences were observed in the case of a high damping ratio when the structural frequency ratio is close to unity.

In practice, the hypothesis of low-level damping is generally implied in the modeling of self-excited forces (Chen and Kareem 2007). In addition, much of the existing bridge is characterized by frequency ratios far from the unity (Bartoli and Mannini 2008). Hence, Eqs. (12) and (13) were rewritten as follows

$$0 = I_1\Omega^3 + I_2\Omega^2 + I_3\Omega + I_4 \approx I_1\Omega^3 + I_3\Omega \tag{14}$$

and

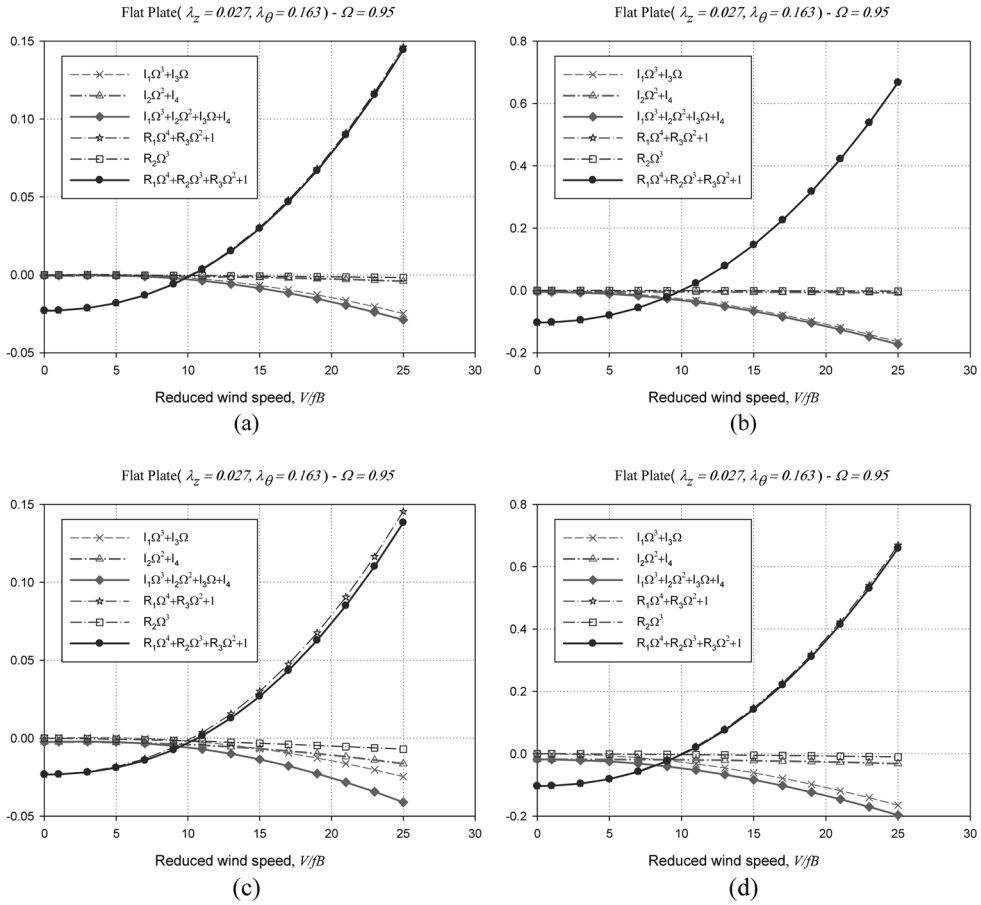

Fig. 3 Variation in R_i, I_i of Flat Plate with *V/fB*:
(a) $\zeta_z = \zeta_\alpha$= 0.0025, γ = 1.17 , (b) $\zeta_z = \zeta_\alpha$ = 0.0025, γ = 1.51,
(c) $\zeta_z = \zeta_\alpha$ = 0.01, γ = 1.17 and (d) $\zeta_z = \zeta_\alpha$ = 0.01, γ = 1.51

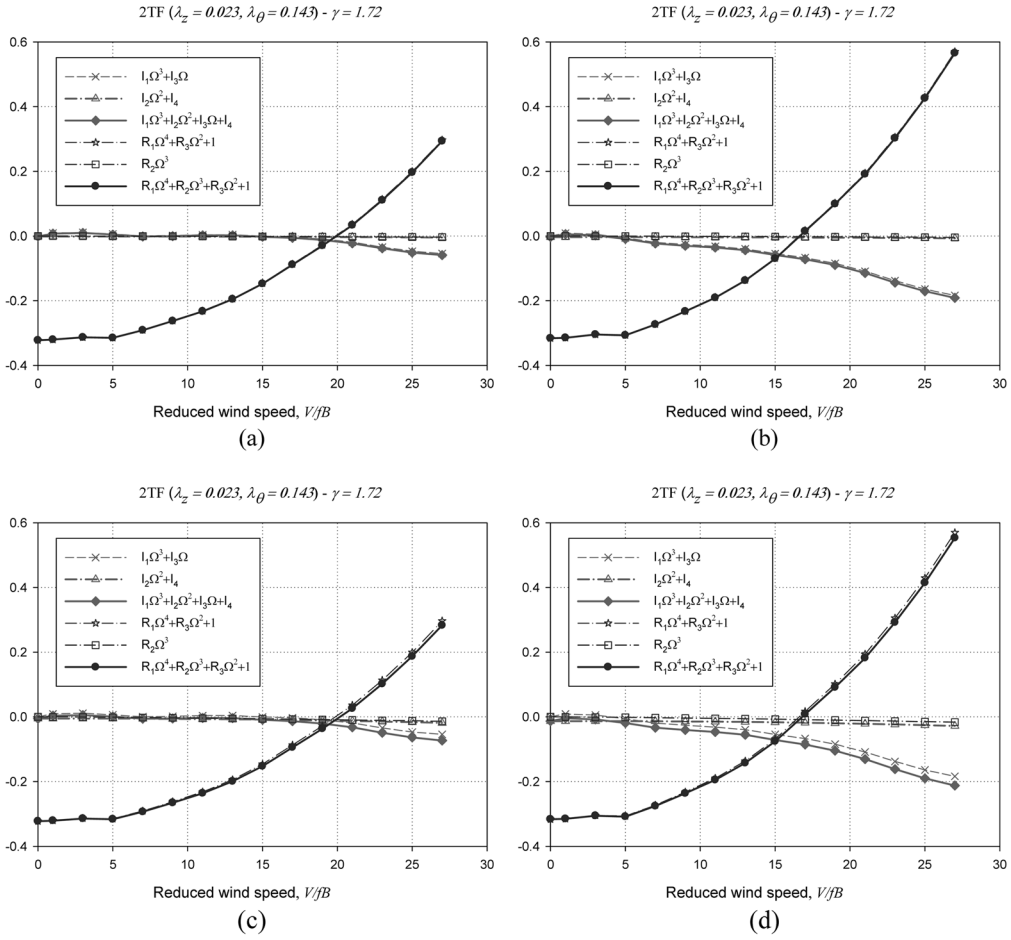

Fig. 4 Variation in R_i, I_i of Flat Plate with V/fB:
(a) $\zeta_z = \zeta_\alpha = 0.0025$, $\Omega = 0.80$, (b) $\zeta_z = \zeta_\alpha = 0.0025$, $\Omega = 0.85$,
(c) $\zeta_z = \zeta_\alpha = 0.01$, $\Omega = 0.80$ and (d) $\zeta_z = \zeta_\alpha = 0.01$, $\Omega = 0.85$

$$0 = R_1\Omega^4 + R_2\Omega^3 + R_3\Omega^2 + 1 \approx R_1\Omega^4 + R_3\Omega^2 + 1 \tag{15}$$

From these equations, Eqs. (21) and (22), an expression for the in-wind frequency ratio Ω^2 can be found

$$\Omega^2 = \frac{(\lambda_z\gamma^2 H_1^* + \lambda_\theta A_2^*)}{\gamma^2[(\lambda_z H_1^* + \lambda_\theta A_2^*) + 0.5\lambda_z\lambda_\theta C_1]} \tag{16}$$

and

$$\Omega_1^2 = \frac{R_3 - \sqrt{R_3^2 - 4R_1}}{2R_1} \qquad \Omega_2^2 = \frac{R_3 - \sqrt{R_3^2 - 4R_1}}{2R_1} \tag{17a, b}$$

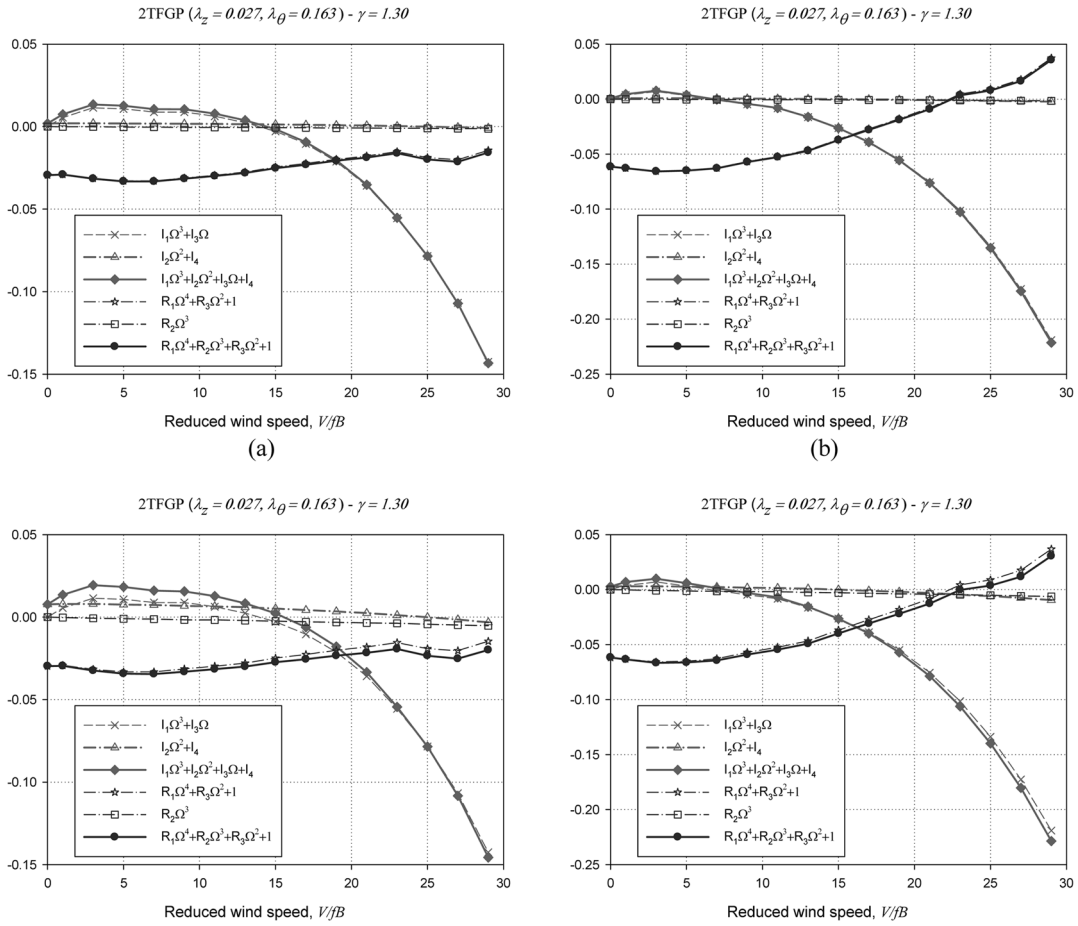

Fig. 5 Variation in R_i, I_i of Flat Plate with V/fB:
(a) $\zeta_z = \zeta_\alpha = 0.0025$, $\Omega = 0.80$, (b) $\zeta_z = \zeta_\alpha = 0.0025$, $\Omega = 0.85$,
(c) $\zeta_z = \zeta_\alpha = 0.01$, $\Omega = 0.80$ and (d) $\zeta_z = \zeta_\alpha = 0.01$, $\Omega = 0.85$

The graphically approximated solution of bimodal flutter problems can easily be found by the intersection point of the Ω^2 root defined by Eq. (16) and Eq. 17(a) or Eq. 17(b) within the respective range of interesting of reduced wind speed, V/fB . It is clear that the curve of $\Omega_1{}^2$ defined the heaving branch coupled flutter, otherwise the curve of $\Omega_2{}^2$ defined the torsional branch coupled flutter. In addition, the intersection point between the curve of $[\Omega^2 - \Omega_i^2](i = 1, 2)$ and the reduced frequency axis V/fB with the lowest value of $V_c / f_c B$ defines the critical flutter wind speed. Fig. 6 illustrates the heaving and torsional branch coupled flutter characteristics of the slotted girder bridge sections of 2*TF* and 2*TFGP* with an angle of attack of 3^0 (Matsumoto *et al*. 2004). It also showed the frequency ratio effects on flutter instability that were obtained by changing the natural frequency of the torsion mode.

On the other hand, it is easy to extract the value of Ω^2 from Eq. (15), then substitute its value in Eq. (16) and by the aid of Eqs. 10(a) and (c) and $\Xi_{ij} = (H_i^* A_j^* - H_j^* A_i^*)(i, j = 1, 2, 3, 4)$, after rearranging some terms, leads to the following expression that could be used to determine the

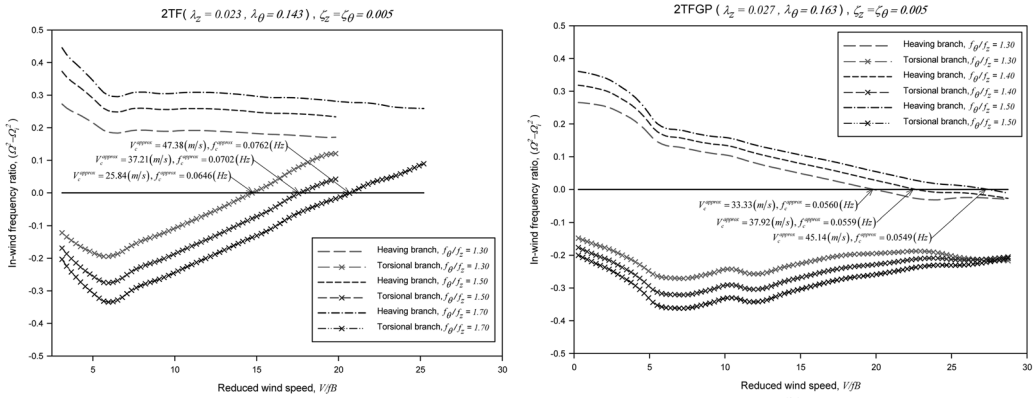

Fig. 6 Coupled flutter analysis for slotted girder section: (a) 2*TF* and (b) 2*TFGP*

critical reduced wind speed

$$
\begin{aligned}
&8\gamma\zeta_z\zeta_\theta(A_2^*\lambda_\theta + H_1^*\lambda_z\gamma^2)[2(A_2^*\lambda_\theta + H_1^*\lambda_z) + \lambda_z\lambda_\theta C_1] \\
&+ \lambda_z^2\lambda_\theta^2\gamma^2[(H_2^*A_4^* + H_3^*A_1^*)C_1 - 2H_1^*A_2^*C_R] + \\
&+ 2\lambda_z\lambda_\theta(1-\gamma^2)\begin{bmatrix} 2H_1^*A_2^*(1-\gamma^2) + (H_2^*A_4^* + H_3A_1)(H_1^*\lambda_z\gamma^2 - A_2^*\lambda_\theta) \\ + 2H_1^*A_2^*(\lambda_\theta A_3^* - \lambda_z\gamma^2 H_4^*) \end{bmatrix} \\
&+ \lambda_z\lambda_\theta^3 A_2^*[A_2^*\Xi_{12} + A_3^*\Xi_{13} + A_4^*\Xi_{32}] + \lambda_z^3\lambda_\theta\gamma^4 H_1^*[H_1^*\Xi_{12} + H_3^*\Xi_{14} + H_4^*\Xi_{42}] = 0
\end{aligned}
\tag{18}
$$

Eq. (18) consists of coupled and uncoupled flutter derivatives that are extracted from the experimental system of 2-DOF sectional models and aerodynamic parameters of the given bridge section. Within the range of interest of reduced velocity, approximated solutions for the critical reduced wind speed and frequency can be found from Eqs. (16) and (18). The results for the four section cases previously investigated are gathered in Table 2, which shows the accuracy of the approximated formulas in estimating the flutter onset frequency and reduced wind speed in the case of low, moderate and high structural damping ratios. The structural frequency ratio assumed for case of the rectangular R15(λ_z = 0.035, λ_θ = 0.174) and Flat Plate (λ_z = 0.027, λ_θ = 0.163) are 1.51 and 1.17, respectively.

It is evident that the results from the approximated formulas are in good agreement in terms of critical frequency solutions with those of the CEA approach. The degree of difference between these proposed formulas and the CEA approach depends on the levels of damping ratio. When the frequency ratio is small and the damping levels are high, as expected, the accuracy of the approximation is inferior. Finally, these approximated formulas give under-predicted results in critical wind speeds.

3.2. Approximated 1-DOF flutter derivatives formulations

A simplified strategy was introduced based on investigating the influence of individual terms on

Table 2 Comparison between the solution of the approximated 2-DOF flutter derivatives formulations and that of CEA

Damping ratio	Onset flutter Error	Flutter derivative set			
		Flat Plate	R15	2TF	2TFGP
$\zeta_z = \zeta_\theta = 0.0025$	V_{rc}^{appox}	15.38	40.81	47.38	33.31
	f_c^{approx}	0.0628	0.1166	0.0762	0.0560
	V_{rc}^{CEA}	16.06	41.78	47.69	34.35
	f_c^{CEX}	0.0625	0.1159	0.0760	0.0558
	ΔV_c (%)	-4.45	-2.36	-0.66	-3.10
	Δf_c(%)	0.45	0.62	0.24	0.38
$\zeta_z = \zeta_\theta = 0.005$	V_{rc}^{appox}	15.41	40.82	47.38	33.33
	f_c^{approx}	0.0627	0.1166	0.0762	0.0560
	V_{rc}^{CEA}	16.71	42.60	47.98	35.29
	f_c^{CEX}	0.0622	0.1153	0.0759	0.0555
	ΔV_c (%)	-8.44	-4.36	-1.26	-5.88
	Δf_c (%)	0.82	1.12	0.46	0.81
$\zeta_z = \zeta_\theta = 0.010$	V_{rc}^{appox}	15.50	40.87	47.41	33.40
	f_c^{approx}	0.0627	0.1166	0.0762	0.0560
	V_{rc}^{CEA}	17.96	44.02	48.55	36.92
	f_c^{CEA}	0.0618	0.1144	0.0756	0.0550
	ΔV_c (%)	-15.81	-7.72	-2.41	-10.55
	Δf_c (%)	1.45	1.89	0.87	1.69

both the imaginary and real parts at certain in-wind frequency ratios when using different damping levels and within a large range of reduced velocities. This strategy leads to a presented approximated method as a result of the previous part.

In this section, we investigate terms related to parameters I_1 from the imaginary part and R_1 from the real part, where coupled and uncoupled flutter derivatives are combined with the ingredients of $0.25\gamma^2\beta C_I$ and $0.25\gamma^2\beta C_R$.

For the several reduced wind speeds V/fB, the terms appearing in the $I_1$and, R_1 are compared in Table 3 for the Flat Plate section, and in Table 4 for the rectangular section $R15$. It is clear that the coefficients of $0.25\gamma^2\beta C_R$ combined with coupled and uncoupled flutter derivatives, are neglected with respect to $\gamma^2[1 + 0.5(\lambda_h H_4^* + \lambda_\alpha A_3^*)]$. Hence, the value of term R_1 in Eq. 10(a) becomes

$$R_1 = \gamma^2\left[1 + \frac{1}{2}(\lambda_z H_4^* + \lambda_\theta A_3^*) + \frac{\lambda_z\lambda_\theta}{4}C_R\right] \approx \gamma^2\left[1 + \frac{1}{2}(\lambda_z H_4^* + \lambda_\theta A_3^*)\right] \quad (19)$$

It is also shown that the coefficients of $0.25\gamma^2\beta C_I$ combined with coupled and uncoupled flutter derivatives are neglected with respect to $0.5\gamma^2(\lambda_h H_1^* + \lambda_\alpha A_2^*)$. Hence, the value of term I_1 in Eq. 11(a) becomes

$$I_1 = \gamma^2\left[\frac{1}{2}(\lambda_z H_1^* + \lambda_\theta A_2^*) + \frac{\lambda_z\lambda_\theta}{4}C_I\right] \approx \frac{\gamma^2}{2}(\lambda_z H_1^* + \lambda_\theta A_2^*) \tag{20}$$

Therefore, Eq. (16) can be rewritten as

$$\Omega^2 = -\frac{I_3}{I_1} = \frac{(\lambda_z\gamma^2 H_1^* + \lambda_\theta A_2^*)}{\gamma^2(\lambda_z H_1^* + \lambda_\theta A_2^*)} \tag{21}$$

Substituting Eq. (21) into Eq. (15) while taking into account Eqs. 10(c) and (19), and after rearranging some terms, leads to the simple equation as follows

Table 3 Variation of terms related to parameters I_1, R_1 with V/fB for Flat Plate (γ= 1.17, λ_z = 0.027, λ_θ = 0.163)

V/fB	$0.25\gamma^2\beta C_I$	$0.5\gamma^2(\lambda_z H_1^* + \lambda_\theta A_2^*)$	I_1	$0.25\gamma^2\beta C_R$	$\gamma^2[1 + 0.5(\lambda_z H_4^* + \lambda_\theta A_3^*)]$	R_1
0	0.0000	0.000	0.000	0.0000	1.368	1.368
3	0.0001	-0.022	-0.022	-0.0004	1.377	1.377
5	0.0002	-0.041	-0.041	-0.0011	1.396	1.395
7	0.0005	-0.066	-0.065	-0.0020	1.428	1.426
9	0.0009	-0.095	-0.095	-0.0032	1.475	1.471
11	0.0012	-0.129	-0.128	-0.0046	1.537	1.532
13	0.0016	-0.167	-0.165	-0.0060	1.615	1.609
15	0.0019	-0.208	-0.206	-0.0073	1.711	1.703
17	0.0022	-0.252	-0.250	-0.0085	1.823	1.814
19	0.0024	-0.299	-0.296	-0.0095	1.953	1.943
21	0.0025	-0.348	-0.346	-0.0102	2.100	2.090

Table 4 Variation of terms related to parameters I_1, R_1, with V/fB for (γ= 1.51, λ_z = 0.035, λ_θ = 0.174)

V/fB	$0.25\gamma^2\beta C_I$	$0.5\gamma^2(\lambda_z H_1^* + \lambda_\theta A_2^*)$	I_1	$0.25\gamma^2\beta C_R$	$\gamma^2[1 + 0.5(\lambda_z H_4^* + \lambda_\theta A_3^*)]$	R_1
0	0.0000	0.000	0.000	0.0000	2.278	2.278
3	-0.0017	-0.094	-0.096	-0.0013	2.347	2.346
5	-0.0037	-0.172	-0.175	-0.0027	2.438	2.435
7	-0.0055	-0.261	-0.267	-0.0038	2.563	2.559
9	-0.0079	-0.361	-0.369	-0.0032	2.712	2.709
11	-0.0117	-0.470	-0.482	0.0002	2.888	2.888
13	-0.0013	-0.614	-0.615	0.0063	3.194	3.201
15	0.0229	-0.780	-0.757	0.0154	3.610	3.625
17	-0.0031	-0.952	-0.955	0.0411	4.168	4.209
19	-0.0147	-1.125	-1.139	0.0563	4.710	4.767
21	0.0078	-1.297	-1.289	0.0377	5.219	5.257

$$(1-\gamma^2)\lambda_z\lambda_\theta[(H_1^*\lambda_z\gamma^2 + A_2^*\lambda_\theta)(A_3^*H_1^* - H_4^*A_2^*) + 2H_1^*A_2^*(1-\gamma^2)]$$
$$+ 8\gamma\zeta_z\zeta_\theta(A_2^*\lambda_\theta + H_1^*\lambda_z\gamma^2)(A_2^*\lambda_\theta + H_1^*\lambda_z) = 0 \quad (22)$$

Eqs. (21) and (22) can be used to estimate the approximated solutions of the critical frequency and reduced wind speed of the combined bridge system. Eq. (21) is the same as the simplified formula for critical frequency proposed by Bartoli and Mannini (2008), which is based on the assumption that the damping ratio is neglected for both bending and torsional modes. These approximated formulas depend on the dynamic parameters of structural bridge: damping ratios $\zeta_i (i = z, \theta)$, structural frequency ratio γ, non-dimensional mass, moment of inertia λ_z, λ_θ, and the aerodynamic parameters: uncoupled flutter derivative A_i (i = 2,3) and H_i (i=1,4) of the given deck bridge section.

The approximations of coefficients R_1 and R_2 are given by Eqs. (19) and (20), respectively. They are considered as reasonable simplifications, if terms C_R and C_I are small amounts to neglect. It can be obtained by utilizing four sets of inter-relationships between coupled flutter derivatives and uncoupled flutter derivatives, which are validated throughout physical measurements for rectangular cylinders as presented in Matsumoto (1996)

$$H_1^* \cong kH_3^*, \qquad H_4^* \cong -kH_2^* \quad (23a, 23b)$$
$$A_1^* \cong kA_3^*, \qquad A_4^* \cong -kA_2^* \quad (23c, 23d)$$

Scanlan *et al*. (1997) shown that the expressions in Eqs. 23(a)-(d) are approximate results for the airfoil case, and some streamlined bridge decks if contribution of A_1^* is very small. Once reductions of the coupled flutter derivative are made in terms R_1 and R_2, Eq. (22) can be derived by equivalent substitutions in the previous simplified flutter equation of real part.

From the aerodynamic point of view, it is noted that Eq. (22) can obtained consistently with the physical phenomenon. Thus, it is not directly derived by setting to zero all the coupled flutter derivatives. Although, all damping and stiffness flutter derivatives still remain in this equation, so it can be concluded that the proposed approximate solutions of critical reduced wind speed for the cross sections are prone to not only the coupled-mode, but also the single-mode flutter (either dominated by torsion or heaving mode).

4. Numerical validations

In this section, numerical computations of the critical reduced wind speed and frequency are performed for a variety of deck sections to validate the degree of approximation as well as to point out the limitations of the approximated approaches that are based on the 1-DOF and 2-DOF flutter derivatives for the combined bridge system. Subsequently, solutions of the CEA for flutter stability are compared between the solutions from Eqs. (16) and (18) [Approx. 2-DOF forms] and Eqs. (21) and (22) [Approx. 1-DOF forms].

4.1. Coupled-mode flutter simulations

Thin flat plate section and the rectangular section of R15 are prone to coupled-mode flutter. Sensitivity

analyses of onset flutter are carried out at both sections for different damping levels and various frequency ratios. Besides that, the results of critical wind speed given by the Selberg (1961) and Rocard (1963) empirical formulas are regarded as reference solutions for case of thin flat plate section.

Results of this analysis are illustrated in Fig. 7 for the rectangular section of R15 (λ_z = 0.027, λ_θ = 0.163) and Fig. 8 for the classical Flat Plate (λ_z = 0.035, λ_θ= 0.174) section. The first conclusion drawn from these graphs for both approximated formulas gives results, which are very close to those obtainable from the solution of the traditional CEA for a wide range of frequency ratios both in the case of structural zero-damping as well as moderate structural damping ($\zeta_z = \zeta_\theta$ = 0.005).

It also shows that when the structural torsional frequency reaches close to the vertical bending frequency, both CEA and Approx. 2-DOF forms shows the critical reduced wind speeds, that tend to become high (Fig. 7) even if approaching infinity (Fig. 8), depending on the type of cross section and structural damping levels. These results are in good agreement with those reported by Dyrbye and Hansen (1997) and Bartoli and Mannini (2008) for the flat plate and rectangular section. Meanwhile, the Approx. 1-DOF forms give opposite results from those of the Approx. 2-DOF forms and the CEA.

Finally, for a thin flat plate the results given by the proposed formula are very similar to those calculated by the empirical Selberg (1961) and Rocard (1963) formulas, as can be seen in Fig. 8, these empirical formulas do not give the infinity critical wind speed when the frequency ratio, γ is very close to unity. However, when the structural torsional frequency is far from vertical bending frequency, all formulas give the same results.

In addition, to validate the accuracy and effectiveness of the proposed approximated approaches, Nine case studies are taken into account, two of which that are reported in Table 5 originate from the existing bridges: case study 3 for the 2nd Geo-Germ Bridge (Larsen 2002) and case study 8 for the Busan-Geoge Grand Bridge (Lee *et al*. 2004). The other case studies show the dynamic parameters of bridges listed in Table 1 and the flutter derivatives set measured from the cross sections prone to the coupled-mode flutter. The geometric and aerodynamic properties of all case studies are listed in Table 5. The solution of critical wind speeds and frequencies calculated from approximated formulations are compared with those of CEA, while approximated results calculated from the Chen and Kareem (2007) and Bartoli and Mannini (2008) formulas are regarded as

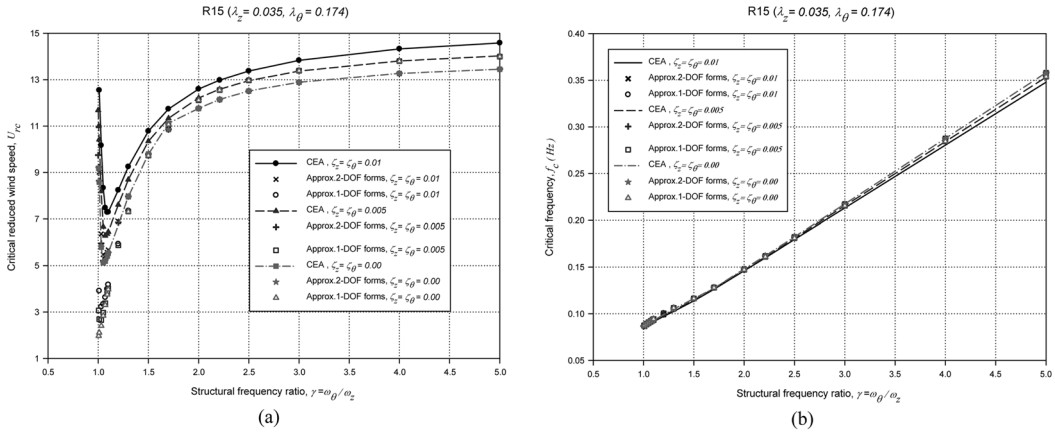

Fig. 7 Comparison of flutter onset of R15 for varying of the structural frequency ratio: (a) critical reduced wind speed and (b) critical frequency

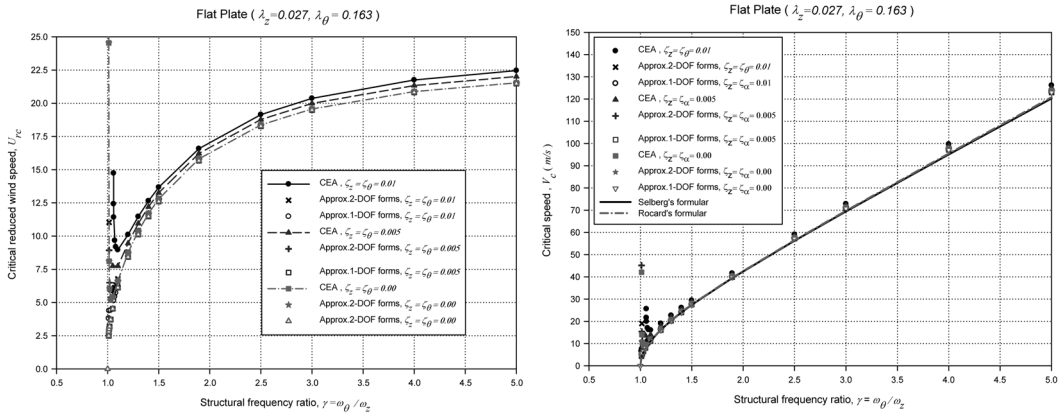

Fig. 8 Comparison of flutter onset of Flat Plate for varying of the structural frequency ratio: (a) critical reduced wind speed and (b) critical wind speed

reference solutions. Finally, all results of these formulas are gathered in the Table 6.

From the results, it can be concluded that both proposed approximated formulations show solutions that are close to those given by the complex eigenvalue analysis, particularly in the flutter frequencies solution. However, when the frequency ratio is less than *1.3*, not only the Approx. 1-DOF forms, but also the Chen and Kareem (2007) and Bartoli (2008) formulas give inaccurate results, as expected (Case 6, Case 7). Meanwhile, the Approx. 2-DOF forms show reasonable results that are in good agreement with those of the CEA in all case studies.

4.2. Single modal flutter simulations

4.2.1. Torsional flutter

A non-streamlined cross section having values of A_2^* tends to change its sign from negative to positive, causing negative aerodynamic damping which will lead to instability in pure torsion (Strømmen 2006). To deal with torsional flutter a mode-by-mode approach is performed, since the resonance frequency associated with this mode is $\omega_\theta(V)$ then $\omega = \omega_\theta(V_{cr})$ and the impedance

Table 5 Case study of coupled-mode flutter simulations

Case study	Flutter derivative set	$B(m)$	$f_z(Hz)$	γ	ζ_z(%)	ζ_θ (%)	λ_z	λ_θ
1	2TF	51.5	0.252	2.64	0.50	0.50	0.0943	0.8727
2	2TF	36	0.232	2.31	1.00	1.00	0.0589	0.5245
3	2nd Geo-Germ	16.9	0.185	2.99	0.30	0.30	0.0305	0.3454
4	2nd Geo-Germ	31	0.099	2.75	0.50	0.50	0.0529	0.4674
5	Flat plate	38	0.204	2.38	0.50	0.50	0.0560	0.9050
6	Flat plate	60.4	0.080	1.32	1.00	1.00	0.0829	0.5942
7	Flat plate	27.5	0.164	1.17	0.20	0.20	0.1815	0.1943
8	Busan-Geoge Grand	22	0.334	3.00	0.50	0.50	0.0225	0.2048
9	R15	13.28	0.465	1.51	0.64	0.64	0.1815	0.1943

Table 6 Results for coupled-mode flutter simulations

Analysis methods	Onset flutter error	Case study								
		1	2	3	4	5	6	7	8	9
Approx. 1-DOF forms	$V_c(m/s)$	274.47	82.57	130.22	106.91	124.65	24.63	19.08	55.39	114.61
	$f_c(Hz)$	0.4509	0.1623	0.4231	0.2008	0.3170	0.0723	0.1895	0.9888	0.5902
	$\Delta V_c(\%)$	-7.98	-6.71	-3.09	-0.18	-3.78	-22.35	-61.13	-8.41	-1.78
	$\Delta f_c(\%)$	-0.71	0.91	2.81	1.57	0.32	1.70	0.35	0.45	0.98
Approx. 2-DOF forms	$V_c(m/s)$	293.82	86.34	131.23	106.59	128.29	27.13	27.98	55.40	112.42
	$f_c(Hz)$	0.4566	0.1630	0.4206	0.1985	0.3188	0.0722	0.1893	0.9708	0.5949
	$\Delta V_c(\%)$	-0.87	-2.05	-2.30	-0.49	-0.84	-11.06	-9.85	-8.40	-3.77
	$\Delta f_c(\%)$	0.54	1.35	2.22	0.43	0.90	1.63	0.2	-1.39	1.77
Chen's forms	$V_c(m/s)$	284.80	86.08	159.75	113.04	126.20	24.78	17.85	89.51	116.92
	$f_c(Hz)$	0.4504	0.1601	0.5540	0.2720	0.3139	0.0713	0.1890	1.0030	0.5848
Bartoli's forms	$V_c(m/s)$	286.48	86.97	134.64	109.96	126.22	24.74	17.69	60.90	119.51
	$f_c(Hz)$	0.4501	0.1608	0.4190	0.2029	0.3137	0.0713	0.1891	0.9858	0.5870
CEA	$V_c(m/s)$	296.38	88.11	134.24	107.11	129.37	30.13	30.74	60.05	116.66
	$f_c(Hz)$	0.4541	0.1608	0.4112	0.1976	0.3160	0.0711	0.1889	0.9843	0.5844

matrix (Eq. (6)) is reduced as follows

$$\boldsymbol{S}_{\eta}\left(\omega_r, V_{cr}\right) = 1 - \kappa_{\theta\theta}^{ae} - \left(\omega_r/\omega_\theta\right)^2 + i2\left(\zeta_\theta - \zeta_{\theta\theta}^{ae}\right)\omega_r/\omega_\theta \tag{24}$$

Setting the real and imaginary parts of Eq. (24) equal to zero, a dynamic stability limit may then be identified at an in-wind resonance frequency

$$\omega_r = \omega_\theta\left(1 + \frac{\rho B^4}{2\tilde{m}_\theta} A_3^*\right)^{-0.5} \tag{25}$$

when the damping properties are

$$\zeta_\theta = \zeta_{\theta\theta}^{ae} = \frac{\rho B^4}{4\tilde{m}_\theta} \times \frac{\omega_r}{\omega_\theta} A_2^*(K_c) \tag{26}$$

Based on a cross section prone to torsional flutter, the sensitivity analyses are also performed to validate the approximation degree of the proposed formulations and 1-DOF Torsion forms Eq. (25) and Eq. (26) that was first presented by Scanlan (Simiu and Scanlan 1996) along with the CEA approach. Let us consider that the previous rectangular section characterized by dynamic properties includes the bridge deck width is B = 35.5 m; non-dimensional mass, moment of inertia are λ_z = *0.035*, λ_θ = *0.174*; fundamental torsional frequency f_θ = 0.192(*Hz*) and the aerodynamics properties of a rectangular cylinder R5 with width to depth ratios of 5 (Matsumoto 1996).

In Fig. 9, the critical reduced wind speed and frequency are plotted against the frequency ratio in the case of zero damping and moderate and high level damping ratios. It is concluded that for the 1-DOF Torsion forms, conservative values of the critical reduced wind speeds are shown when

structural frequency ratios are changed. Meanwhile, both the critical frequency and reduced velocity curves defined by the Approximated 1-DOF and 2-DOF formulations show the same trend as that of CEA. When the frequency ratios are close to unity, the Approx. 2-DOF forms show the peak value of critical reduced velocity. Nevertheless, the errors between solution of the approximated formulations and that of CEA are observed in case of high-level damping.

Further numerical validation of the case studies presented in Table 7 is provided at the end of this section, where one case study is of the existing structure, the Seohae Grand bride (Case 5), and the other case studies are of the Edge-girder bridge sections combined with the prototypes of the geometric parameters of the existing bridges such as Busan-Geoge Grand (Case1, Case 3), Golden Gate (Case 2, Case 6), Kärkinen (Case 4) and the aerodynamics parameters of the rectangular section of R5, R10 with width to depth ratios of *5, 10* (Matsumoto 1996).

From the results gathered in Table 8, it seems possible to conclude that both proposed approximate formulas give results that agreed well with those of CEA as well as with those of the Bartoli and Mannini (2008) and Chen and Kareem (2007) formulas. For the case of the Golden Gate bridge, characterized by a very small frequency ratio ($\gamma = 1.17$), not only the Approx. 1-DOF forms but also reference formulas show poor accuracy results when compared with the those of CEA, while the Approx. 2-DOF forms still give accurate results (Case 2, Case 6).

4.2.2. Heaving-mode aeroelastic instability

A cross section having bluffness with values of H_1^* tends to change its sign from the negative to positive causing negative aerodynamic damping which will lead to instability in pure bending (Strømmen 2006). Since the resonance frequency associated with this mode is $\omega_z(V)$ then $\omega_r = \omega_z(V_{cr})$ and the impedance matrix (Eq. (6)) becomes

$$\boldsymbol{S}_\eta(\omega_r, V_{cr}) = 1 - \kappa_{zz}^{ae} - (\omega_r/\omega_z)^2 + i2(\zeta_z - \zeta_{zz}^{ae})\omega_r/\omega_z \tag{27}$$

Setting the real and imaginary parts of this equation equal to zero, when the damping properties are

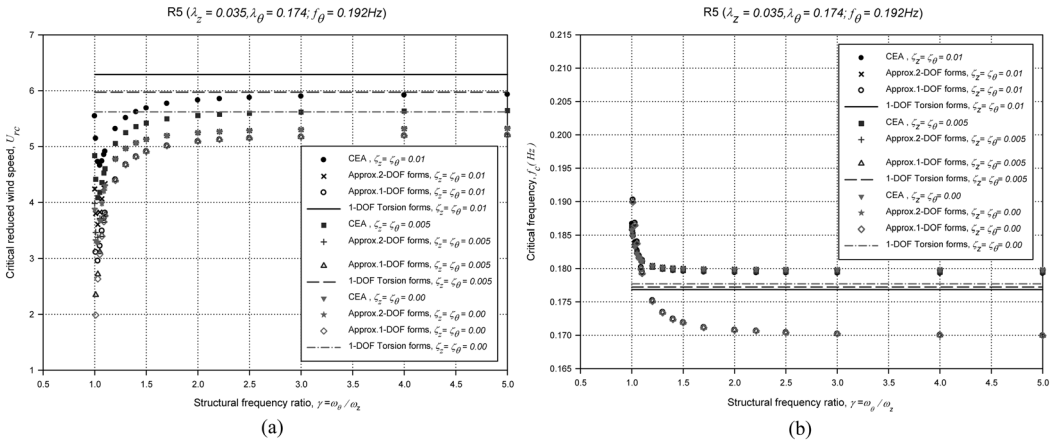

Fig. 9 Comparison of flutter onset of R5 for varying of the structural frequency ratio
(a) critical reduced wind speed and (b) critical frequency

Table 7 Case study of torsional flutter simulations

Case study	Flutter derivative set	$B\,(m)$	$f_z(Hz)$	γ	$\zeta_z(\%)$	$\zeta_\theta(\%)$	λ_z	λ_θ
1	R5	22	0.334	3.00	0.5	0.5	0.0225	0.2048
2	R5	27.5	0.164	1.17	0.5	0.5	0.1815	0.1943
3	R10	22	0.334	3.00	0.5	0.5	0.0225	0.2048
4	R10	13.28	0.465	1.51	0.64	0.64	0.0128	0.1270
5	Seohae Grand	34	0.250	1.84	0.5	0.5	0.0502	0.6061
6	Seohae Grand	27.5	0.164	1.17	0.5	0.5	0.1815	0.1943

Table 8 Results for torsional flutter simulations

Analysis methods	Onset flutter error	Case study					
		1	2	3	4	5	6
Approx. 1-DOF forms	$V_c(m/s)$	109.23	15.29	158.15	69.29	45.72	15.81
	$f_c(Hz)$	0.8674	0.1833	0.8247	0.6182	0.4165	0.1861
	$\Delta V_c(\%)$	-5.86	-28.85	-6.43	-10.48	-4.00	-21.09
	$\Delta f_c(\%)$	-6.46	1.83	-8.58	-5.24	-1.08	-0.05
Approx. 2-DOF forms	$V_c(m/s)$	110.37	20.10	160.57	70.33	46.57	17.72
	$f_c(Hz)$	0.9290	0.1800	0.9083	0.6579	0.4215	0.1869
	$\Delta V_c(\%)$	-4.87	-6.46	-4.99	-9.13	-5.26	-8.04
	$\Delta f_c(\%)$	0.19	0.02	0.69	0.84	0.31	0.38
1-DOF Torsion forms	$V_c(m/s)$	118.95	28.62	179.84	85.19	52.52	18.68
	$f_c(Hz)$	0.9121	0.1752	0.8535	0.6327	0.4110	0.1851
Chen's forms	$V_c(m/s)$	117.70	20.15	169.56	77.61	51.88	15.46
	$f_c(Hz)$	0.9270	0.1802	0.8983	0.6520	0.4600	0.1916
Bartol's forms	$V_c(m/s)$	113.27	10.02	165.88	76.96	48.23	17.02
	$f_c(Hz)$	0.9306	0.1853	0.9069	0.6580	0.4275	0.1868
CEA	$V_c(m/s)$	116.02	21.49	169.01	77.39	47.55	19.15
	$f_c(Hz)$	0.9273	0.1800	0.9021	0.6524	0.4210	0.1862

$$\zeta_z = \zeta_{zz}^{ae} = \frac{\rho B^4}{4\tilde{m}_\theta} \times \frac{\omega_r}{\omega_z} H_1^* \tag{28}$$

a dynamic stability limit may then be identified at an in-wind resonance frequency

$$\omega_r = \omega_z \left(1 + \frac{\rho B^2}{2\tilde{m}_z} H_4^*\right)^{-0.5} \tag{29}$$

As shown in Fig. 10, the critical reduced velocity and frequency of the previous rectangular section ($\lambda_z = 0.035$, $\lambda_\theta = 0.174$) with the fundamental vertical bending frequency $f = 0.087(Hz)$ and the aerodynamics properties of a rectangular cylinder with width to depth ratios of 1 ($B/D = 1$), R1 (Matsumoto 1996) obtained by the approximated approaches or CEA are compared for various frequency ratios under different damping levels. It seems possible to conclude that the Approx. 2-

DOF forms and 1-DOF Bending forms Eqs. (28) and (29) show results that agree fairly well with those obtained by the CEA method.

Table 9 shows that the case studies of the prototypes using the flutter derivative set of R1, R2 are rectangular prisms with $B/D = 1,2$ and have heaving divergent type instability (Matsumoto 1996) and the geometric parameters of the previous bridge are listed in Table 1. Table 10 summarizes the results of the critical reduced velocity and frequency using the proposed formulas and the conventional CEA and 1-DOF Bending forms.

From the results, the differences in the critical flutter speed and frequency given by the proposed Approx. 2-DOF forms and CEA are between three and five percent. Meanwhile, it seems that when the frequency ratio is greater than *1.5*, the approximate 1-DOF forms are sufficient to obtain an acceptable accuracy.

5. Conclusions

In this paper, a set of simplified formulations for estimating flutter critical and frequency has been proposed. Firstly, a properly simplified strategy is used by neglecting some damping ratio terms in coefficients of the real and imaginary equation part of flutter equation, as the results, approximated formulas, consist of the uncoupled and coupled flutter derivatives are derived. These formulas are able to show accurate results when compare with those obtain by CEA method, even if structural close unity in case of low damping level. Furthermore, the characteristics of the torsional branch (TB) and heaving branch (HB) are also highlighted in order to easily identify in which branch the coupled flutter instability occurs because the frequency ratio, Ω for TB and HB is asymmetric in terms of torsional and heaving motion.

Next, when the non-dimensional mass and polar moment of inertia coefficients associated with flutter derivatives are neglected, the simplified formulations are to be compacted of the uncoupled flutter derivatives (H_1^*, H_4^* and A_2^*, A_3^*) . These uncoupled flutter derivatives could be extracted from the one-degree-of freedom test set-up. This assumption is in agreement with the inter-relationship among flutter derivatives (Matsumoto 1996), which seems to be suitable for the flutter

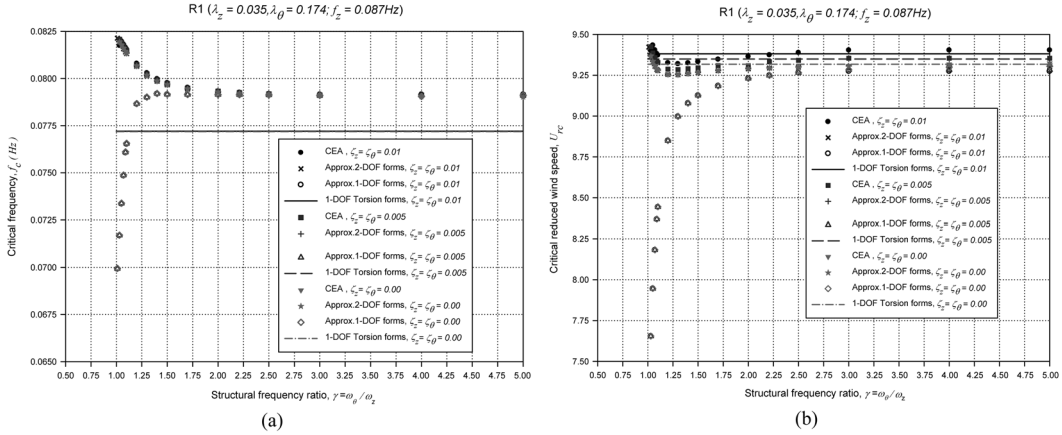

Fig. 10 Comparison of flutter onset of R1 for varying of the structural frequency ratio
(a) critical reduced wind speed and (b) critical frequency

Table 9 Case study of heaving-mode aeroelastic instability simulations

Case study	Flutter derivative set	$B(m)$	$f_z(Hz)$	γ	$\zeta_z(\%)$	$\zeta_\theta(\%)$	λ_z	λ_θ
1	R1	22	0.334	3.00	0.50	0.50	0.0225	0.2048
2	R1	13.28	0.465	1.51	0.64	0.64	0.0128	0.1270
3	R1	34	0.250	1.35	0.50	0.50	0.0502	0.6061
4	R2	22	0.334	3.00	0.50	0.50	0.0225	0.2048
5	R2	13.28	0.465	1.51	0.64	0.64	0.0128	0.1270
6	R2	27.5	0.164	1.17	0.50	0.50	0.1815	0.1943

Table 10 Results for heaving-mode aeroelastic instability simulations

Analysis methods	Onset flutter error	Case study					
		1	2	3	4	5	6
Approx. 1-DOF forms	$V_c(m/s)$	64.00	54.44	52.78	56.81	58.34	8.26
	$f_c(Hz)$	0.3137	0.4479	0.1973	0.2391	0.4048	0.1703
	$\Delta V_c(\%)$	-0.97	-2.77	-27.17	-7.74	-4.76	33.37
	$\Delta f_c(\%)$	-0.03	-0.29	-13.67	-11.43	-2.21	-3.11
Approx. 2-DOF forms	$V_c(m/s)$	64.20	55.25	72.14	60.51	59.05	6.18
	$f_c(Hz)$	0.3137	0.4489	0.2283	0.2726	0.4128	0.1671
	$\Delta V_c(\%)$	-0.66	-1.31	-0.46	-1.74	-3.59	-0.21
	$\Delta f_c(\%)$	-0.03	-0.08	-0.11	0.95	-0.27	-4.93
1-DOF Bending forms	$V_c(m/s)$	63.96	55.84	66.27	55.49	56.35	7.53
	$f_c(Hz)$	0.3105	0.4463	0.2087	0.2333	0.3911	0.1699
CEA	V_c (%)	64.62	55.99	72.47	61.58	61.25	6.19
	f_c (%)	0.3138	0.4492	0.2285	0.2700	0.4139	0.1758

derivatives of a wide range of cross-section geometries, hence the physical consistency is still guaranteed in the approximate formulations. Besides that, its accuracy was verified for a variety of bridge cross sections showing that the approximate solutions in onset flutter is acceptable when structural frequency is larger than *1.5*, wherein first torsion mode and vertical bending mode are enough far from each other.

Finally, the pragmatic feature of these approximate formulations is that they are able to capture all aerodynamic instabilities such as coupled-mode flutter as well as single-mode-dominated flutter cases where the previous empirical as well as approximate formulas are no longer applicable.

Acknowledgments

The support of the research reported here by the grant from the Ministry of Land, Transport and Maritime Affairs of Korean Government through Super Long Span Bridge R&D Center is gratefully acknowledged.

References

Bartoli, G. and Mannini, C. (2008), "A simplified approach to bridge deck flutter", *J. Wind Eng. Ind. Aerod*., **96**(2), 229-256.
Bleich, F. (1949), "Dynamic instability of truss-stiffened suspension bridge under wind action", *Proc. ASCE*, **74**(8), 1269-1314.
Chen, X and Kareem, A. (2007), "Improved understanding of bimodal coupled bridge flutter based on closedform solutions", *J. Struct. Eng*., **133**(1), 22-31.
D'Asdia, P. and Sepe, V. (1998), "Aeroelastic instability of long span suspended bridges: a multimode Approach", *J. Wind Eng. Ind. Aerod*., **74-76**, 849–857.
Dyrbye, C. and Hansen, S.O. (1997), *Wind Loads on Structures*, Wiley, New York.
Korea Highway Corporation (KHC). (1998), "Wind tunnel report for the Seohae Grand bridge", Kyunggi-do, Korea.
Kiviluoma, R. (2001), "Frequency-domain approach for calculating wind induced vibration and aeroelastic stability characteristics of long span bridges". PhD thesis, Acta Polytechnica Scandinavica.
Larsen, A. (1993), "Aerodynamic aspects of the final design of the 1624m suspension bridge across the Great Belt", *J. Wind Eng. Ind. Aerod.*, **48**(2-3), 261-285.
Larsen S.V. (2002), "Section model tests for the design of the 2nd Geo-Germ Bridge", Force Technology-DMI, Lyngby, Denmark.
Lee, H.E., *et al*. (2004), "Section model tests for the design of the cable stayed bridge, Lot1, Busan-Geoge Fixed Link", Korea University Research Centre for Disaster Prevention Science and Technology, Seoul, Korea
Livesey, F.M. (1995), "Wind tunnel studies of the Hoga Kusten Bridge during construction, Part II: Aeroelastic model tests", DMI Report 94124, Danish Maritime Institute, Denmark.
Matsumoto, M. (1996), "Aerodynamic damping of prisms", *J. Wind Eng. Ind. Aerod.*, **59**(2-3), 159-175.
Matsumoto, M. (1999), "Recent study on bluff body aerodynamics and its mechanism", *Proceedings of the10th Int. Conf. on Wind Engineering, Wind Engineering into the 21st Century*, (Eds., A. Larsen, G.L. Larose, and F.M. Livesey), Balkema, Rotterdam, The Netherlands.
Matsumoto, M., Shijo, S., Eguchi, A., Hikida, T., Tamaki, H. and Mizuno, K. (2004), "On the flutter characteristics of separated two box girders", *Wind Struct.*, **7**(4), 281-291.
Nakamura, Y. (1978), "An analysis of binary flutter of bridge deck sections", *J. Sound Vib.*, **57** (4), 471-482.
Nissen, H.D., Sørensen, P.H. and Jannerup, J. (2004), "Active aerodynamic stabilisation of long suspension bridges", *J. Wind Eng. Ind. Aerod*., **92**(10), 829-847.
Rocard, Y. (1963), "Instabilite des ponts suspendus dans le vent-experiences sur modele reduit", *Nat. Phys. Lab. Paper*, **10**, England.
Sarkar, P.P., Jones, N.P. and Scanlan, R.H. (1992), "System identification for estimation of flutter derivatives", *J. Wind Eng. Ind. Aerod.*, **42**(1-3), 1243-1254.
Scott, R. (2001), In the wake of tacoma, suspension bridges and the quest for aerodynamics stability, American society of civil engineers, reston VA.
Selberg, A. (1961), "Oscillation and aerodynamic stability of suspension bridges", *Acta. Polytech. Scand*., **13**, 308-377
Scanlan, R.H. and Tomko, A. (1971), "Airfoil and bridge deck flutter derivatives", *J. Eng. Mech,-ASCE*, **97**(6), 1717-1737.
Scanlan, R.H., Jones, N.P., and Singh, L. (1997), "Inter-relation among flutter derivatives" , *J. Wind Eng. Ind. Aerod*., **69-71**, 829-837.
Strømmen, E. (2006), *Theory of Bridge Aerodynamics*, Springer Verla Publications.
Simiu, E. and Scanlan, R.H. (1996), *Wind Effects on Structures*, Wiley, New York.
Theodorsen, T.(1934), "General theory of aerodynamic instability and the mechanism of flutter", Technical Report. 496, N.A.C.A., Washington, 413-433
Yang, Y.X., Ge, Y.J and Cao, F.C. (2007), "Flutter performance of central-slotted box girder section for Long span suspension Bridges", *China J. Highway & Transport*, **20**(3), 35-40.
Yang, Y.X., Ge, Y.J. (2009), "Aerodynamic flutter control for typical girder sections of long-span cable-supported bridges", *Wind Struct*., **12**(3), 205-217.
Zhang X.J. (2006), "Study of design parameters on flutter stability of cable-stayed-suspension hybrid bridges",

Wind and Structures", *Wind Struct*., **9**(4), 331-344.
Zhou, L. and Ge, Y.J. (2009), "Sectional model test study on vortex-excited resonance of vehicle-bridge system of Shanghai Bridge over Yangtse River", *Frontiers of Arch. & Civil Eng. in China*, **3**(1), 67-72.

CC